ACS Sustainable Chemistry & Engineering

Article

Increase of ceria redox ability by lanthanum addition on Ni based catalysts for hydrogen production

Cristina Pizzolitto, Federica Menegazzo, Elena Ghedini, Giada Innocenti, Alessandro Di Michele, Giuseppe Cruciani, Fabrizio Cavani, and Michela Signoretto

ACS Sustainable Chem. Eng., **Just Accepted Manuscript** • DOI: 10.1021/acssuschemeng.8b02103 • Publication Date (Web): 04 Oct 2018

Just Accepted

ACS Publications

is published by the American Chemical Society. 1155 Sixteenth Street N.W., Washington, DC 20036

Increase of ceria redox ability by lanthanum addition on Ni based catalysts for hydrogen production

Cristina Pizzolitto,[a] Federica Menegazzo,[a] Elena Ghedini,[a] Giada Innocenti,[b] Alessandro di Michele,[c] Giuseppe Cruciani,[d] Fabrizio Cavani,[b] Michela Signoretto[a]*

a Ms C. Pizzolitto, Dr. F. Menegazzo, Dr. E. Ghedini, Prof. M. Signoretto, CATMAT Lab, Department of Molecular Sciences and Nanosystems, Ca' Foscari University Venice and INSTM RU of Venice, via Torino 155, I-30172 Venezia Mestre, Italy E-mail: miky@unive.it

b Ms G. Innocenti, Prof. F. Cavani, Department of Industrial Chemistry "Toso Montanari", University of Bologna, viale Risorgimento 4, I-40136 Bologna, Italy and Consorzio INSTM, UdR di Bologna, Firenze, Italy

c Dr. A. Di Michele, Department of Physics and Geology, University of Perugia, Via Pascoli 1, I-06123, Perugia, Italy

d Prof. G. Cruciani Department of Physics and Earth Sciences, University of Ferrara, Via Saragat 1, I-44100 Ferrara, Italy

KEYWORDS Ni catalysts; ethanol steam reforming; DRIFT-MS; CeO_2; La_2O_3

ABSTRACT The effects of lanthanum addition in Ni/CeO_2 catalysts were investigated. The influence of synthetic procedures, namely impregnation or co-precipitation of lanthanum and cerium oxide, were evaluated. Materials were analyzed by BET, AAS, DRIFT-MS, TPR, OSC, XRD and SEM-EDX. Samples were tested in Ethanol Steam Reforming (ESR). Both lanthanum-promoted samples exhibited a higher stability in time than non-promoted catalyst. Nonetheless,

catalytic behavior is strongly affected by the preparation method. TPR, OSC and XRD analyses showed that co-precipitation method allowed the best interaction between ceria and lanthana, leading to an increased redox ability and best catalytic performances as a result. A catalyst with a support prepared via co-precipitation method showed ethanol conversion of 90% and hydrogen selectivity higher than 70% even after 60 hours of reaction.

Introduction

Nowadays, most of the energy demand is fulfilled by fossil sources [1] that, despite their high efficiency, suffer from environmental and social problems, on top of them the enormous impact on greenhouse effect [2]. In this scenario, hydrogen is considered as the energy carrier of the future, since it is a clean source of energy that can be used inside fuel cells as a feed for electric engines [3]. Actually, longer-term strategies of car manufacturers are devoted to develop and to commercialize electric vehicles based on hydrogen fuel cells, and some of them have already put these cars into the open market [4]. However, hydrogen presents multiple set of problems regarding its transport and storage. A possible solution of this strategy is to reform liquid biofuels inside the car, producing hydrogen that can be directly consumed by electrochemical reaction inside the cell, supplying energy. Solid Oxide Fuel Cells (SOFCs) have received great attention in the last years because they are composed of all solid components, they can work at high operating temperature conditions and they don't suffer from CO poisoning. Moreover, SOFCs have an even greater feature: its anode can also be used for direct internal reforming of hydrocarbons (DIR-SOFC) [5-8], so its use can avoid hydrogen problems. Methane is more commonly used as a reforming substrate [9], but reforming of non-fossil fuel sources is highly expected. Biomass utilisation has received considerable interest for its great potentialities: in fact

it can be employed for the production of hydrogen [10, 11]. Ethanol is an interesting biofuel because it can be obtained from the fermentation of biomass, avoiding fossil sources problems. Ethanol can be transformed via Ethanol Steam Reforming (ESR) into hydrogen ($CH_3CH_2OH + 3\ H_2O \leftrightarrows 6\ H_2 + 2\ CO_2$). However, one of the big issues of this system is coke deposition on the catalyst, due to the undesired reactions involved in the ESR conditions. For this reason, it is necessary to use a catalyst that could control the process and at the same time could work as possible anode for electrolytic reaction. Moreover, it must be stable against carbon deposition onto its surface and thermal stress [12]. For this purpose, heterogeneous catalysts are commonly used for ESR [13]. The most active metals for this kind of reactions are the noble ones, in particular, platinum, palladium and rhodium [14]. However, due to their high cost, noble metals are less attractive for industrial applications. Nickel is the most efficient substitute and is the most used metal in industrial field [15]. Two of its main drawbacks are sintering and deactivation. For this reason, support has a crucial role on the reaction to overcome nickel limitations, leading to high stability, activity and resistance for the process [16, 17]. The typically used supports for this kind of reaction are alumina, silica, ceria and zirconia. Ceria is an attractive one because it's also widely employed as anode inside fuel cells [18]. Therefore, in the present work, the authors chose ceria as support because it shows oxygen storage capacity that is linked to its facility to transport the vacancy from the surface to the bulk of the system, changing structural shape from CeO_2 to Ce_2O_3 [19]. In this way, the oxygen vacancies could promote the oxidation of carbonaceous species on the surface, limiting coke deposition [20, 21]. Because of this feature, ceria is normally used in CO oxidation reaction, preferential oxidation (PROX) of CO for hydrogen purification, water gas shift (WGS) reaction and many other reactions [22]. Moreover, ceria redox ability can be modulated by a careful control of structural defects: the

highest is the number of defective sites, the most effective is the redox pump. For this reason, many studies focused the attention on ceria modification by the substitution of cerium with heteroatoms of different chemical nature. Laguna *et al.* described how oxygen vacancies population are increased by introducing Fe^{3+} inside ceria lattice [23], while Andana *et al.* used Cu^{2+} [24]. Lanthanum oxide could be an innovative promoter in this sense. In fact, La^{3+} could substitute Ce^{4+} on support lattice, increasing its redox ability [25]. The similar dimension of ionic radii (La^{3+} = 1.16 Å and Ce^{4+}= 0.97 Å) could facilitate the interaction between the two elements. Moreover, lanthanum oxide is a structural promoter, with high mechanical strength that could increase ceria stability at high temperatures [26]. These catalytic systems, based on nickel+ceria+lanthanum, could be very interesting for many catalytic applications, such as for example glycerol steam reforming and for the reforming with carbon dioxide rather than steam (CH_4/CO_2 reforming). In the present work, the attention was focused on the investigation of lanthanum addition in Ni/ceria catalysts for ESR process. In particular, the aim is the development of an innovative heterogeneous catalyst that is selective and robust towards coke deposition. The influence of synthetic procedures, such as impregnation or co-precipitation of lanthanum and cerium, was evaluated.

Results and Discussion

Preliminary characterizations

The choice of two synthetic methodologies allowed investigating if there are differences in materials physicochemical properties and thus different lanthanum promotional effect on catalytic performances. In particular, lanthanum impregnation over ceria (Ni-La-Ce) and lanthanum co-precipitation together with ceria (co-Ni-La-Ce) were investigated. First,

preliminary characterizations were performed. N_2 adsorption-desorption measurements were carried out in order to quantify the specific surface area and pore size distribution of the catalysts and in order to evaluate the possible effects of lanthanum addition on surface properties of final material. This aspect is of crucial importance in heterogeneous catalyst because it is known that a high surface area greatly improves the dispersion of the active phase and the interaction between metal and reagents [27]. Figure 1 represents the adsorption-desorption isotherms (upper part) and BJH distributions (lower part) of Ni-Ce, Ni-La-Ce and co-Ni-La-Ce catalysts, while Table 1 summarizes the corresponding data.

Table 1: Specific surface area, pore size distribution and pore volume for Ni-Ce, Ni-La-Ce and co-Ni-La-Ce catalysts.

	Ni-Ce	Ni-La-Ce	co-Ni-La-Ce
Surface area (m^2/g)	106	66	76
Pore average diameter (nm)	6	5	4
Pore volume (cm^3/g)	0.10	0.02	0.03

The three samples exhibit a IV-type isotherm, according to IUPAC classification, with the characteristic hysteresis loop typical of mesoporous materials. For Ni-Ce catalyst, this loop is located at higher V_{ads} values than for Ni-La-Ce and co-Ni-La-Ce, indicating the higher surface area. Both samples containing lanthanum have lower surface area values, calculated by BET method, and lower pore volumes than non-doped ceria catalyst. Such result is in agreement with data obtained for lanthanum promotion on SBA-15 [28]. The decrease in surface area of ceria material after the addition of lanthanum could be due to two different effects. In the case of Ni-

La-Ce sample, lanthanum is introduced into CeO_2 after the calcination process in which ceria structure is already built. For this reason, the shape of the hysteresis is the same of the not promoted sample and the only difference is the lower surface area. This decrement is due to the block of pore by the introduction of lanthanum and nickel via impregnation method. On the contrary, in the case of co-Ni-La-Ce, lanthanum and ceria are co-precipitated together. This means that the structure of ceria is influenced by the presence of lanthanum during precipitation. For this reason, both the shape and the position of the hysteresis are different from the previous catalysts.

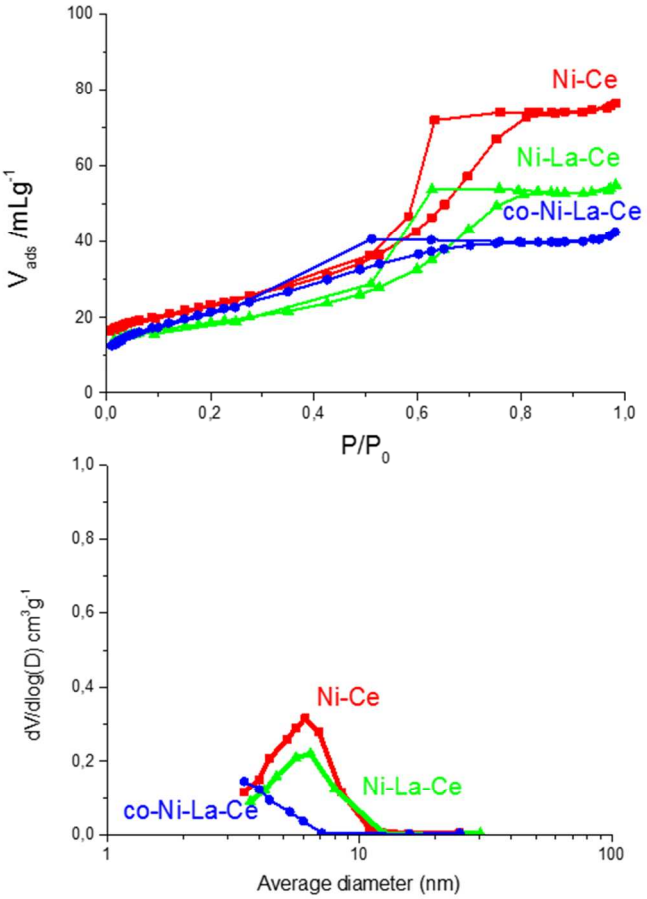

Figure 1: N_2 adsorption/desorption isotherms (upper part) and BJH curves (lower part) of Ni-Ce (■), Ni-La-Ce (▲) and co-Ni-La-Ce (●) catalysts.

Atomic adsorption analyses were carried out in order to quantify the effective nickel amount in the catalysts. As expected, since nickel was introduced by incipient wetness impregnation, all catalysts present the nominal metal amount, which is 8 wt %.

Reactivity tests

ESR tests were conducted monitoring reaction mixture tipically for 16 hours. Figure 2 (section a) reports ethanol conversion against time of reaction for the three catalysts. The corresponding products distribution for the three samples, and ethanol conversions plus hydrogen yields are reported in Table 2. A stability test of 60 hours for the best sample, which is co-Ni-La-Ce catalyst, is also shown in Figure 2 (section b).

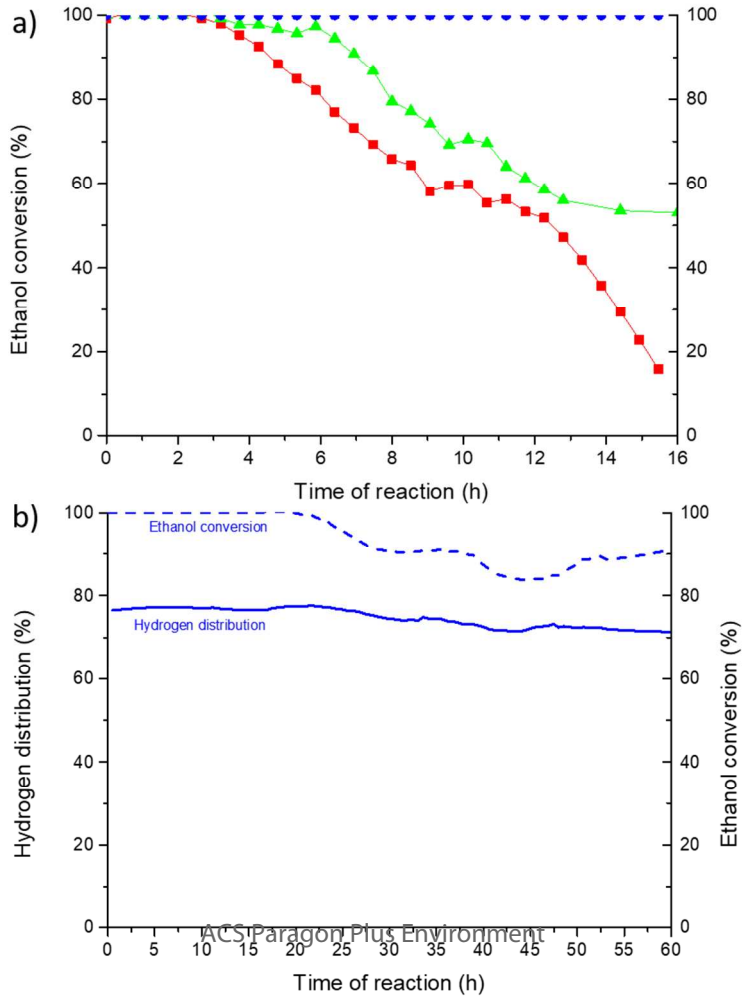

Figure 2: Ethanol conversion for Ni-Ce (■), Ni-La-Ce (▲) and co-Ni-La-Ce (●) (section a); Stability test of co-Ni-La-Ce catalyst for 60 hours (section b).

It should be highlighted that none of the three catalysts shows carbon monoxide in the products (Table 2). This result has a crucial importance: the absence of CO means that water gas shift reaction is favored ($CO + H_2O \leftrightarrows CO_2 + H_2$); in fuel cell applications, CO is commonly a poison, even if SOFCs are more tolerant to this gas because they can oxidize it to CO_2 at the anode ($CO + O^{2-} \leftrightarrows CO_2 + 2e^-$). At the same time, at low temperature CO could lead to coke formation, through the Boudouard reaction ($2CO \leftrightarrows C + CO_2$). For this reason, direct oxidation of CO to CO_2 in SOFCs is important to limit coke deposition [29] and therefore a low or even null CO production is a promising result. Considering catalytic behavior over time (Figure 2), non-doped Ni-Ce catalyst presents a steady decrease in ethanol conversion, reaching the value of 25 % after 16 hours of reaction. The sample presents a high hydrogen yield only for the first hours of reactions, showing a gradual decrease from 70 % to 20 % through 16 hours. As it is

possible to see from the catalytic results, by lanthanum incorporation into ceria, there is an increase of both hydrogen yield and ethanol conversion after 16 hours of reaction. However, catalytic results strongly indicate that preparation method deeply affects the development of a stable and active catalyst: the same promoter does not lead to the same catalytic result. The best performances were obtained when lanthanum oxide was added via co-precipitation method (Figure 2 and Table 2). Such sample maintains an ethanol conversion of 100 % for at least 16 hours of reaction, due to the experimental conditions used.

Table 2: Hydrogen yield, ethanol conversion and product distribution of Ni-Ce, Ni-La-Ce and co- Ni-La-Ce after 16 hours of reaction.

	Ni-Ce	Ni-La-Ce	co-Ni-La-Ce
EtOH conv (%)	33	55	100
H_2 yield (%)	18	37	70
H_2 distribution (%)	70	69	76
CH_4 distribution (%)	2	10	3
CO_2 distribution (%)	28	21	21
CO distribution (%)	0	0	0

100 % of conversion is not significantly relevant to understand the behavior of a catalyst, so to further prove the increment in the redox effect and, as a consequence, in the stability of co-Ni-La-Ce catalyst, a prolonged test was performed (60 hours). In Figure 2 (section b) ethanol conversion and hydrogen distribution of co-Ni-La-Ce are presented. It is possible to see that, during this prolonged time on stream, conversion is 100% for the first twenty hours, and then there is a small and gradual decrease. A deactivation effect is shown, which probably also occurs during the initial 20 hours at which ethanol conversion is complete. Conversion is still 90 % at

the end of the sixtieth hour. At the same time, hydrogen distribution is almost constant for all the time on stream.

Another important aspect is the reducibility of the catalysts in the reaction environment. In order to have a deep knowledge of the interaction between ethanol and catalytic surface, DRIFT-MS technique was performed.

Figure 3 shows DRIFTS spectra of pure support (Ce), Ni-Ce and co-Ni-La-Ce recorded while exposing the catalysts continuously to pure ethanol at different temperatures. The spectrum of pure support is used as reference and a more deepened description of the spectrum can be found in the supplementary materials. In the case of Ni-Ce and co-Ni-La-Ce catalysts, not significant differences are visible at RT, and even the trends shown when the temperature was raised were similar in the two cases. Indeed, bands differed only slightly in terms of wavenumber ($\Delta\nu < 5$ cm-1) for the two samples. As far as Ni-Ce sample is concerned, ethanol was adsorbed on the catalyst surface at RT as both undissociated molecule and ethoxide [30, 31]. The presence of H-bonded ethanol is corroborated by two broad bands, one from 3100 to 3500 cm^{-1} and the other centered at 1236 cm^{-1}. The ethoxy is adsorbed in two different modes, as bidentate (1060 cm^{-1}) and monodentate (1104 cm^{-1}) [32]. The bands at 2970, 2926, 2898, 2869, 1445 and 1381 cm^{-1} are related to ethoxy $\nu as(CH_3)$, $\nu as(CH_2)$, $\nu s(CH_2)$, $\nu s(CH_3)$, $\delta as(CH_3)$ and $\delta s(CH_3)$, respectively. The catalyst terminal OH group were characterized by the negative $\nu(OH)$ at 3660 cm^{-1}. As far as the band at 1236 cm^{-1} is concerned, the assignation is not unambiguous since the other H-bonded ethanol characteristic band is detected up to 150 °C.

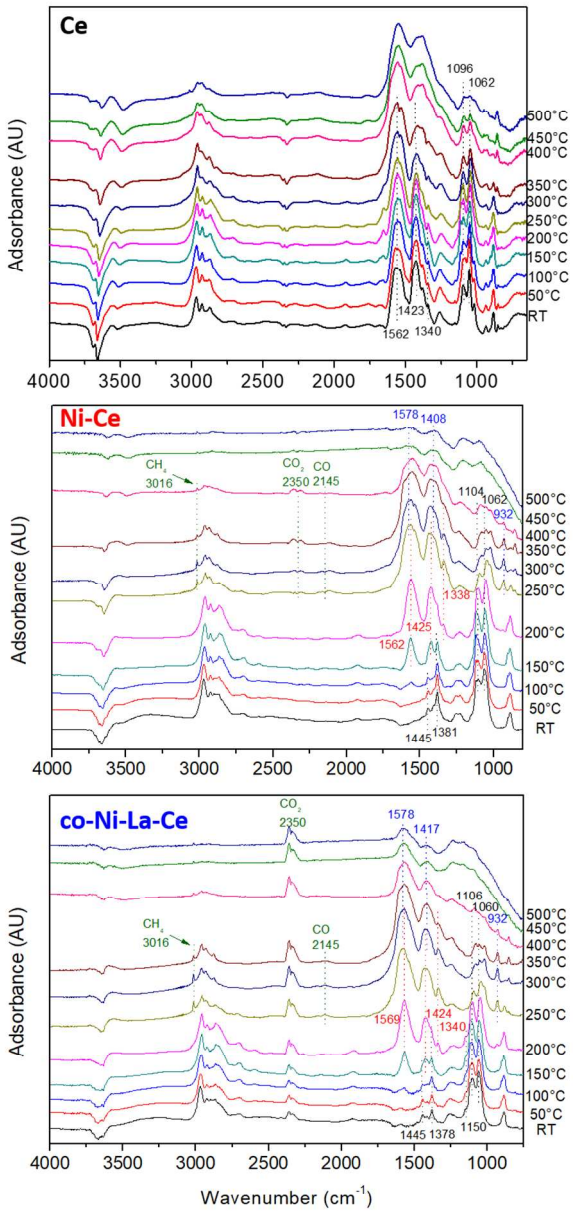

Figure 3: DRIFTS analyses of Ce, Ni-Ce and co-Ni-La-Ce samples feeding ethanol at different temperatures.

Ethanol was continuously fed, hence, it might be reasonable to hypothesize that some un-dissociated ethanol might interact with the catalyst surface even at higher temperatures but it is possible to find the η2-acetaldehyde ν(C-O) at the same wavenumber [30]. The presence of the

latter is corroborated, for co-Ni-La-Ce sample, by the shoulder at 1150 cm^{-1} assignable to η2-acetaldehyde ν(C-C) visible even at RT. Unfortunately, it is not possible to distinguish unambiguously any shoulder in the Ni-Ce spectra (nor at RT neither at higher temperatures) and hence for this sample the assignation can be only uncertain. At 150 °C, the acetates ναs(COO) and νs(COO) started to be completely detectable at 1562 cm^{-1} and 1429 cm^{-1}, respectively. The acetate band intensities increase raising the temperature and at 200 °C the acetate δ(CH_3) appeared at 1338 cm^{-1} [33]. A further temperature increase led to the appearance of some bands due to bridged and bidentate carbonates (928 cm-1 and 1021 cm-1, respectively) [34]. The broadening of COO acetates bands is due to their convolution with the carbonates ones until 400 °C. From 250 °C to 400 °C three gas phase bands were detected at 3018 cm^{-1}, 2338 cm^{-1} and 2140 cm^{-1} assignable to CH_4, CO_2 and CO respectively. In correspondence of these bands appearance, the MS experiment showed a maximum in CO, CH_4, H_2 and acetaldehyde (the MS trends are reported in Figure S2 in the ESI). Xu et al. [33] detected a decrease of the acetate band intensities and observed the disappearance of ethoxy species at high temperatures. In our case, we do not see such a decrease in acetate or ethoxy surface species due to their continuous formation from the ethanol stream. It is also important to notice that Xu et al correlated NiO reduction by ethanol with high temperatures (250°C-400°C) using XRD analysis. Moreover, in those experiments the spectrum base line underwent to a dramatic drop down under 1500 cm^{-1} from 400 °C to 500 °C, associated to NiO reduction [35]. It is possible to state that ethanol reduces NiO ($CH_3CH_2OH + NiO \rightarrow CH_3CHO + Ni^0 + H_2O$) since no H_2 was produced before 250 °C. In fact, its production started along with the vanishing of η2-acetaldehyde peaks. Indeed, CO and CH_4 showed an absolute maximum between 250 °C and 350 °C since they are the products of acetaldehyde decomposition, whose MS trend did not show a definite maximum. The

fact that water trend reached its minimum during the NiO reduction, while it should be coproduced, might be due to the catalyst H_2O adsorption as indicated by the small broad band clearly detected at 3579 cm^{-1} from 250 to 350 °C associated with the formation of new O-H bond. Furthermore, the water release decrement, in this temperature range, might be due to its consumption in the steam reforming reaction that started at 250 °C as shown by the ethanol MS trend. The water trend increases after 350 °C might be due to the release of water by the catalyst surface as suggested by the OH band diminution. Further information given by the MS analysis are reported in the ESI. Overall, it was possible to demonstrate that in the reaction conditions herein reported a catalyst pre-reduction is not necessary, since ethanol, acting as a reducing agent, is able to rapidly activate the catalytic system.

Influence of lanthanum on nickel reducibility

TPR analyses were performed in order to identify how the support influences NiO reducibility (Figure 4, continuous lines) and to check ceria reducibility (Figure 4, dotted lines). Focusing on catalysts' TPR profiles (continuous line), Ni-Ce's profile shows a peak centred at 260 °C which is ascribable to the NiO species that weekly interact with ceria, and another one at 340 °C, due to NiO species with the support more strongly. It can be underlined that the introduction of lanthanum via impregnation method leads to a shift of the peaks to higher temperatures (by 20 °C and 40 °C respectively), indicating an increase in metal-support interaction strength. On the contrary, lanthanum introduction via co-precipitation method slightly affects the interaction strength between ceria and NiO; therefore, no evident differences for this sample are visible. Moreover, TPR analyses are even more important for the interpretation of ceria reducibility. For this reason, H_2-TPR analysis of bare supports have been performed (Figure 4 underlined line). Two different peaks can be observed: the first one, centered around 500 °C, is associated with

the reduction of surface ceria from Ce^{4+} to Ce^{3+}; the second peak, located around 800 °C is connected with the reduction of the bulk support [36, 37]. Since the reaction has to be performed at 550 °C, the first peak assumes a fundamental importance to understand the reducibility of the system under reaction conditions. As regards the lanthanum doped samples, it is possible to underline a shift, for both peaks, to lower temperatures. Such shift is an indication that the introduction of lanthanum makes ceria more reducible, which can help to improve oxygen mobility during the reforming reaction, as reported by Dong *et al.* [38]. Such difference in ceria reducibility is the first tool to understand the catalytic results and explain the higher stability of lanthanum doped samples. Mobile oxygen species take part to the oxidation of carbon species, limiting coke deposition over catalyst surface and implementing its stability during the reaction.

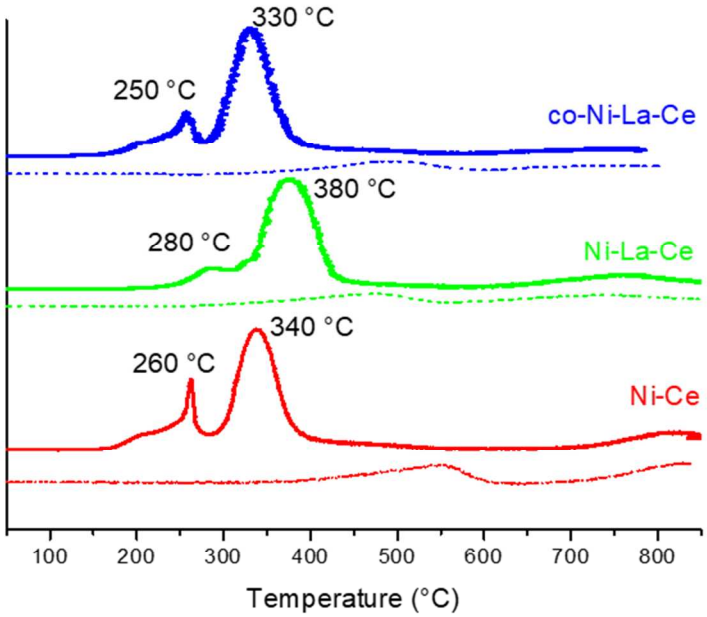

Figure 4: TPR profile of pure supports (underline lines) and Ni-Ce, Ni-La-Ce and co-Ni-La-Ce (continuous lines)

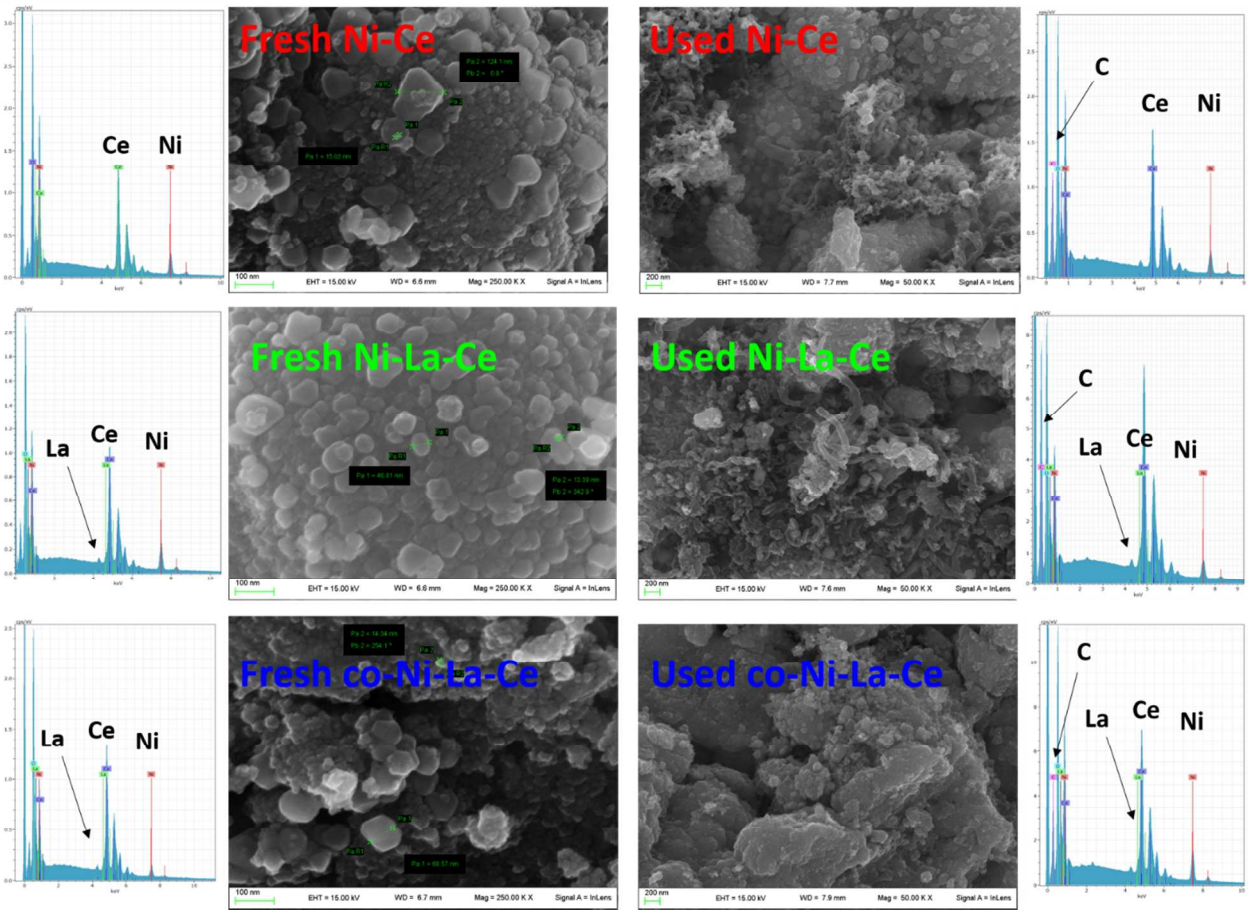

Figure 5: SEM and EDX analyses of fresh (left) and used (right) ceria supported catalysts.

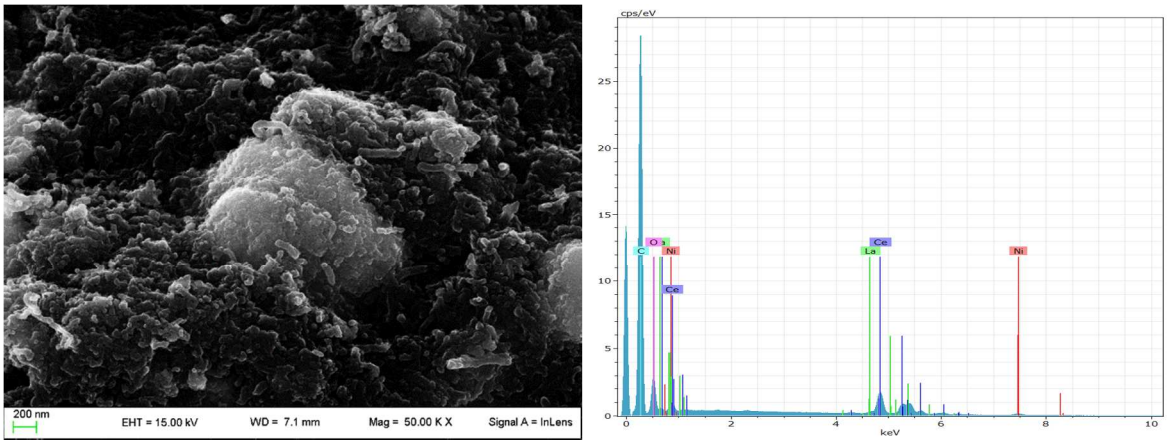

Figure 6: SEM and EDX analyses of co-Ni-La-Ce spent after 60 hours of reaction.

Influence of lanthanum on catalyst structure

FE-SEM analyses of fresh catalysts and the corresponding EDX analyses are shown in Figure 5 (left). It is possible to affirm that nickel is well and homogeneously dispersed on ceria surface of the three samples as it's visible in the nickel mapping reported in the top part of Figure 7.

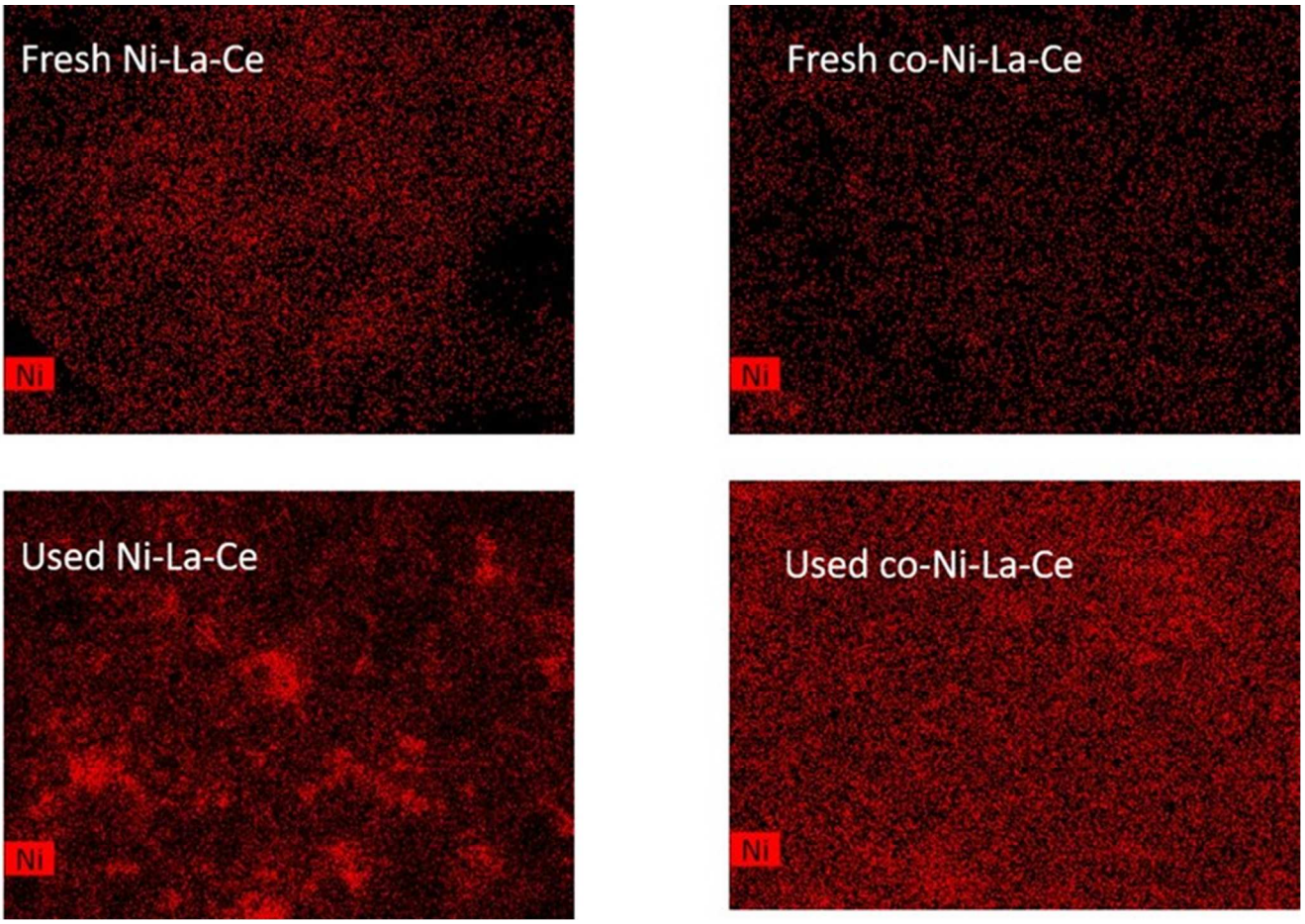

Figure 7: Representative Nickel mapping images by EDX-SEM of Ni-La-Ce fresh and used (left) and co-Ni-La-Ce fresh and used (right)

The dimension of ceria particles is around 90 nm. A rough determination of nickel particle size shows that the three samples exhibit nickel nanoparticles in the range 10-15 nm. XRD analyses

were carried out in order to identify the ceria crystal phase, the nickel phase and to determine more carefully the nickel mean size (Figure 8). These analyses were conducted in the reduced samples in order to get as much closer to reaction conditions as possible, despite the reduction of NiO is carried out by the oxidation of ethanol to acetaldehyde in the reaction environment, as it has been demonstrated by DRIFT technique. In the three catalysts, a fluorite-type structure of ceria is present with characteristic peaks at 2 theta 28 °, 33 °, 47 °, 56 ° and 59 ° associated with (111), (200), (220), (311) and (222) of cubic phase, respectively [39, 40].

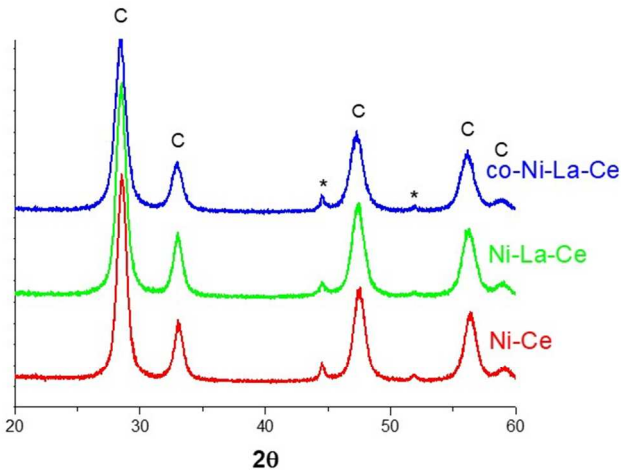

Figure 8: XRD analysis of reduced ceria supported samples (C is the ceria crystal phases and * is Ni° species).

The characteristic peak at 2 theta 43,4 ° and 52,0 ° indicates that nickel is present in its metallic phase and they are respectively associated with (111) and (200) Miller Indexes of fcc nickel [41] By means of the Rietveld method, it was calculated the mean size of Ni^0: 17 nm for Ni-Ce, 10 nm for Ni-La-Ce and 14 nm for co-Ni-La-Ce. Lanthanum in this case influences the nickel particle size, leading to a slight decrease of its dimension. Usually, in this kind of reactions, the smallest is the size, the highest is the catalyst stability [42, 43]. In fact, the most active catalysts

for this reaction are those promoted with lanthanum, which have a smaller nickel particle size than non-doped sample.

Furthermore, the XRD technique was used to analyze the ceria cell parameters to investigate the lanthanum effect on ceria support. Table 3 reports cell parameters for the catalysts where a_0 and V_0 refer to the unit-cell constant and the unit-cell volume, respectively, of the Ni-Ce sample.

For the two lanthanum-doped samples, it can be seen an increase in unit-cell constant and unit-cell volume, in particular for the catalyst synthesized with the co-precipitation method. The increase in the unit-cell volume can be taken as a strong evidence that lanthanum is fully hosted as La^{3+} ions (ionic radii 1.16 Å) replacing Ce^{4+} ions (ionic radii 0.97 Å) in the ceria lattice. This is also in perfect agreement with the absence of any diffraction peak related to metallic lanthanum or lanthanum oxide(s) in the XRD patterns of Ni-La-Ce and co-Ni-La-Ce samples (see Figure 8). A likely explanation is that the substitution of two Ce^{4+} with two La^{3+} atoms can be balanced with an oxygen vacancy. This could bring to an increase in redox ability. This property could improve the ability to oxidize carbonaceous species on the surface, limiting the deactivation due to coke formation and stabilizing the catalyst. In fact, we have shown that co-Ni-La-Ce is the best performing catalyst and presents a very good stability.

Table 3: Variation of lattice parameters of the catalysts and oxygen storage capacity of supports.

		Ni-Ce	Ni-La-Ce	co-Ni-La-Ce
XRD	V/V_0	1	1,006	1,012
	a/a_0	1	1,002	1,004
		Ce	La-Ce	co-La-Ce
OSC	mmol O_2/g	0,13	0,58	0,77

The redox ability of a material can be accurately assessed using the Oxygen Storage Capacity method (OSC). In this case, the three supports, and not the final catalysts, were analyzed. In fact, the method allows understanding the capacity of support oxygen adsorption, and this is directly proportional to its redox abilities. Ceria adsorbed the lowest amount of oxygen (mmol of O_2 per grams), while there is an increment of O_2 adsorption passing from the impregnated support (La-Ce) to the co-precipitated one (co-La-Ce) (Table 3). Also this characterization technique demonstrates the effects on ceria redox ability of both lanthanum addition and synthetic methodology. In fact, promoter addition, in particular by co-precipitation, leads to an increase of OSC, which means an increase in ceria redox ability and therefore an increase in stability towards coke poisoning.

To further confirm the results, SEM analyses of used catalyst have been made. Figure 5 (right) shows SEM imagines and EDX analyses of catalysts after 16 hours of reaction, while Figure 6 reported SEM image and EDX analysis of co-Ni-La-Ce after 60 hours of reaction. Looking at

Figure 5, the differences between used samples are evident. Used Ni-Ce surface is completely covered by small nanotubes, while used Ni-La-Ce shows few nanotubes with diameter size around 44 nm. As for co-Ni-La-Ce catalyst, no nanotube species are detected on the surface of used sample, and only small percentage of carbonaceous species (5-6%) is depicted by EDX analysis. The same catalyst was tested for 60 hours and, looking at SEM and EDX analyses of spent catalyst (Figure 6) it is possible to observe the presence of coke on the catalyst surface. However, coke does not cover the whole surface and in particular, it is still possible to observe the Ni nanoparticles. This could explain the good activity of the catalyst after 60 hours of reaction but also its partial deactivation.

Furthermore, Figure 7 represents nickel mapping images of used promoted samples (after 16 hours of reaction) in order to highlight the reasons for different deactivation of these two catalysts. Used co-Ni-La-Ce presents a homogeneous distribution of nickel particles while for used Ni-La-Ce sporadic particle agglomeration is evident. As reported in introduction, lanthanum insertion into ceria could enhance the support redox ability and both mechanical and thermal stability. For Ni-La-Ce catalyst the preparation method strongly affects its mechanical and thermal stability and the lesser La^{3+} substitution in ceria lattice gives lower redox ability at the system in comparison with co-Ni-La-Ce. The combination of these two effects does not allow the stabilization of nickel particle on the surface and, as it is evident for used Ni-La-Ce in Figure 8, nickel sintering is visible. This result is in agreement with the data previously discussed.

Conclusions

The effects of lanthanum addition in nickel ceria samples was investigated in order to find a stable, active and resistant catalyst for ethanol steam reforming. Our results highlight that lanthanum introduction method strongly affects the catalytic performances. Lanthanum co-precipitation allows a stronger interaction between La^{3+} and Ce^{4+} than impregnation, and this is evident by Rietveld unit cell refinements. This strongest interaction leads to the highest oxygen mobility in ceria bulk, as observed by OSC analysis and TPR. This property has a beneficial effect on the oxidation of carbonaceous species during the reaction and leads to a prolonged stability of the catalyst during the reaction. In fact, lanthanum added via co-precipitation leads to the best performances, 100 % ethanol conversion and 70 % hydrogen distribution after 16 hours of reaction. No nanotube species are depicted in SEM images of used catalyst. Moreover, no nickel sintering is visible. In addition, for this catalyst it was performed a prolonged test. It was found that, after 60 hours, ethanol conversion is still 90% and hydrogen distribution is higher than 70%. Such catalytic system, based on nickel+ceria+lanthanum, could be very interesting also for many other catalytic applications, such as for example, glycerol steam reforming and dry reforming.

Experimental

Synthesis of supports

Ceria support (denoted as Ce) was synthesized by precipitation from $(NH_4)_2Ce(NO_3)_6$ (Sigma Aldrich) by urea at 100 °C in aqueous solution. The solution was mixed and boiled for 6 h at 100 °C, the precipitate was washed in boiling deionized water and dried at 110 °C for 18 hours. The material was then calcined under air flow (30 mL/min) at 550 °C for 3 hours. Lanthanum oxide was introduced on the support using two different methods: incipient wetness impregnation and

co-precipitation with the support. In the former case (denoted as La-Ce support), the proper amount of $La(NO_3)_3*6H_2O$ was added to the calcined support in order to obtain obtain 5 wt% of lanthanum on the final catalyst. The material was dried at 110 °C in the oven and then calcined in flowing air (30 mL/min) at 550 °C for 3 hours. In the latter method (denoted as co-La-Ce support), the same amount of $La(NO_3)_3*6H_2O$ was dissolved together with the support precursor and the synthetic methodology was as previously described for non-promoted ceria.

Synthesis of catalysts

The metal introduction on the support was performed by incipient wetness impregnation with a proper amount of $Ni(NO_3)_2*_{6H2O}$ aqueous solution in order to obtain 8 wt % of nickel on the material. After drying at 110 °C for 18 hours, calcination was performed under air flow (30 mL/min) at 550 °C for 4 hours.

The samples are labelled:

Ni-Ce

Ni-La-Ce introduction of lanthanum via impregnation method.

co-Ni-La-Ce introduction of lanthanum via co-precipitation method.

Characterizations

Surface areas and pore size distributions were obtained from N_2 adsorption/desorption isotherms at -196 °C (using a Micromeritics ASAP 2000 analyser). Surface area was calculated from the N_2 adsorption isotherm by the BET equation [44], and pore size distribution was determined by the BJH method [45]. Total pore volume was taken at $P/P_0 = 0.99$.

Nickel amount was determined by atomic adsorption spectroscopy (AAS) after microwave disaggregation of the samples (100 mg) using a Perkin-Elmer Analyst 100.

DRIFT-MS analyses were measured by an IR apparatus Bruker Vertex 70 equipped with a Pike DiffusIR. Spectra were recorded using a MCT detector after 128 scans and 4 cm-1 resolution. The mass spectrometer was an EcoSys-P from European Spectrometry Systems. The samples were pretreated at 500 °C in He flow (8 ml/min) for 60 min, and then the bare catalyst IR spectra were collected every 50 °C from 500 °C to room temperature (RT). Afterwards, ethanol was fed at 0.6 μL min-1 and, as the ethanol mass signal started to raise, the RT spectrum was recorded. Sample temperature was then increased by 5 °C/min and spectra were collected every 50 °C. The adsorbed species spectra were obtained at each temperature by subtracting the catalyst spectrum at the proper temperature.

Temperature programmed reductions (TPR) were carried out in a lab-made equipment: samples (50 mg) were heated with a temperature rate of 10 °C/min from 25 °C to 800 °C in a 5 % H_2/Ar flow (40 mL/min). The effluent gases were analysed by a TCD detector and by a Genesys 422 quadrupole mass analyzer (QMS).

Oxygen Storage Capacity (OSC) analyses were carried out in the same lab-made equipment used for TPR. 50 mg of sample were pre-treated in H_2 flow (40 mL/min) until 550 °C and maintained at this temperature for 1 hour. Then the sample was purged in He flow and cool down to 25 °C. Pulses of a 5% O_2/He mixture where carried out until TCD signal saturation.

X-ray powder diffraction (XRD) patterns were measured by a Bruker D8 Advance diffractometer equipped with a Si(Li) solid state detector (SOL-X) and a sealed tube providing Cu K radiation. The Rietveld refinement method as implemented in the Bruker TOPAS

programme was used to obtain the refined unit cell parameters, crystal size, and the quantitative phase analysis for the supports and metal phases in the samples. The crystal size determination is achieved by the integral breadt based calculation of volume weighted mean crystallize sizes assuming intermediate crystallite size broadening modelled by a Voigt function. The samples were reduced in H_2 flow for 1 h at 550 °C before the analysis and then passivated in air flow at 25 °C.

FE-SEM images were obtained using a Field Emission Gun Electron Scanning Microscopy LEO 1525 ZEISS, after metallization with Chromium. The images were acquired by InLens detector while elemental composition was determined using Bruker Quantax EDS (resolution of 2 nm at 20 kV).

Catalytic tests

The catalytic tests were performed with a PID microactivity-Effi reference reactor (Process Integral Development Eng&Tech) coupled to a gas-chromatograph (HP 6890) and to a Genesys 422 quadrupole mass analyzer (QMS). Microactivity-Effi reactor is an automatic and computerized high-pressure catalytic reactor which includes valves and process layout inside a hot box to avoid possible condensation of volatile products, while also preheating the reactants efficiently. Using a HPLC pump (Gilson 303) the mixture of water and ethanol (molar ratio 6:1) was flowing and helium was used as carrier. The total amount of molar flow was 0,615 mol/h considering a molar ratio composition of 91,75% of He, 1,20 % of Ethanol and 7,23 % of Water. The typical reaction temperature was 550 °C. Preliminary tests were performed without the catalyst and using the bare supports. No evident ethanol conversion has been observed in these experiments at the typical reaction temperature. Samples were charged inside the reactor without

a preliminary reduction; this allows skipping one step, turning out to be more economically convenient for industrial applications. In fact, the catalyst is reduced in situ by the reactive mixture as it was demonstrated by DRIFT technique.

After the analysis, conversion of ethanol, product distribution and hydrogen yield were calculated using the following equations:

Conversion of ethanol:

$$\text{Conversion (\%)} = 100\% - (f_{\text{out}}(\text{EtOH}))/(f_{\text{in}}(\text{EtOH}))*100\%$$

Product distribution:

$$\text{Product distribution (\%)} = (f_{i\ \text{out}})/(\sum[\![f_{i\ \text{out}}]\!])*100\%$$

Hydrogen yield:

$$\text{Hydrogen yield (\%)} = (fH_{2\ \text{out}})/(6*f\text{EtOH}_{\text{in}})*100\%$$

where f is the flow in mol/min.

To have a homogenous catalyst, tablets were pressed and grained to obtain the ideal grain size range (0,3-0,4mm). Afterwards the catalyst (150 mg) was mixed with siliciumcarbide (SiC, VWR, ratio catalyst:SiC=1:4 by volume). The catalysts were not reduced before reaction.

Supporting information

Mass analyses of both support and catalysts feeding ethanol and the hypothesized surface pathways are reported in Supplementary Information.

Corresponding Author

* Prof. M. Signoretto, CATMAT Lab, Department of Molecular Sciences and Nanosystems, Ca' Foscari University Venice and INSTM RU of Venice, via Torino 155, I-30172 Venezia Mestre, Italy E-mail: miky@unive.it

Author Contributions

The manuscript was written through contributions of all authors. All authors have given approval to the final version of the manuscript.

Funding Sources

MIUR-Italy (PRIN2015); Fondazione Cassa di Risparmio di Perugia for financial support. (Project Code: 2016.0106.021).

ACKNOWLEDGMENT

Financial support to this work by MIUR-Italy (PRIN2015) is gratefully acknowledged. Dr. Di Michele thanks Fondazione Cassa di Risparmio di Perugia for financial support. (Project Code: 2016.0106.021).

REFERENCES

[1] Foster, E.; Contestabile, M.; Blazquez, J.; Manzano, B.; Shah, M.N. The unstudied barriers to widespread renewable energy deployment: Fossil fuel price responses. Energy Policy 2017, 103, 258–264, DOI 10.1016/j.enpol.2016.12.050.

[2] Mundaca, G. How much can CO_2 emissions be reduced if fossil fuel subsidies are removed?. Energy Economics 2017, 64, 91–104, DOI 10.1016/j.eneco.2017.03.014.

[3] Steil, M.C.; Nobrega, S.D.; Georges, S.; Gelin, P.; Uhlenbruck, S.; Fonseca, F.C. Durable direct Ethanol anode-supported solid oxide fuel cell. Appl. Energy 2017, 199, 180–186, DOI 10.1016/j.apenergy.2017.04.086.

[4] Ball, M.; Weeda, M. The hydrogen economy-vision or reality?. Int. J. Hydrogen Energy 2015, 40, 7903-7919, DOI 10.1016/j.ijhydene.2015.04.032.

[5] Qu, J.; Wang, W.; Chen, Y.; Deng, X.; Shao, Z. Stable direct-methane solid oxide fuel cells with calcium-oxide-modified nickel-based anodes operating at reduced temperatures. Appl. Energy 2016, 164, 563–571, DOI 10.1016/j.apenergy.2015.12.014.

[6] Shiratori, Y.; Sakamoto, M. Performance improvement of direct internal reforming solid oxide fuel cell fuelled by H_2S-contaminated biogas with paper-structured catalyst technology. J. Power Sources 2016, 332, 170-179, DOI 10.1016/j.jpowsour.2016.09.095.

[7]Ormerod, R.M. Solid oxide fuel cells. Chem. Soc. Rev. 2003, 32, 17–28, DOI 10.1039/B105764M

[8] da Silva, A.A.A.; Bion, N.; Epron, F.; Baraka, S.; Fonseca, F.C.; Rabelo-Neto, R.C.; Mattos, L.V.; Noronha, F.B. Effect of the type of ceria dopant on the performance of Ni/CeO_2 SOFC anode for ethanol internal reforming. Appl. Catal., B 2017, 206, 626–641, DOI 10.1016/j.apcatb.2017.01.069.

[9] Florea, M.; Matei-Rutkovska, F.; Postole, G.; Urda, A.; Neatu, F.; Pârvulescu, V.I.; Gelin, P. Doped ceria prepared by precipitation route for steam reforming of methane. Catal. Today, 2018, 306, 16-171, DOI 10.1016/j.cattod.2016.12.006.

[10] Amin, R.; Liu, B.S.; Zhao, Y.C.; Huang, Z.B. Hydrogen production by corncob/CO_2 dry reforming over CeO_2 modified Ni-based MCM-22 catalysts. Int. J. Hydrogen Energy 2016, 41, 12869-12879, DOI 10.1016/j.ijhydene.2016.05.233.

[11] Ketzer, D.; Rosch, C.; Haase, M. Assessment of sustainable Grassland biomass potentials for energy supply in Northwest Europe. Biomass Bioenergy, 2017, 100, 39-51, DOI 10.1016/j.biombioe.2017.03.009.

[12] Luo, J.Z.; Yu, Z.L.; Ng, C.F.; Au, C.T. CO_2/CH_4 reforming over Ni-La_2O_3/5A: an investigation on carbon deposition and reaction steps. J. Catal. 2000, 194, 198–210, DOI 10.1006/jcat.2000.2941.

[13] Kubacka, A.; Fernandez-Garcia, M.; Martinez-Arias, A. Catalytic hydrogen production through WGS or Steam reforming of alcohols over Cu, Ni and Co catalysts. Appl. Catal., A 2016, 518, 2-17, DOI 10.1016/j.apcata.2016.01.027.

[14] Nematollahi, B.; Rezaei, M,; Khajenoori, M. Combined dry reforming and partial oxidation of methane to synthesis gas on noble metal catalysis. Int. J. Hydrogen Energy 2011, 36, 2969-2978, DOI 10.1016/j.ijhydene.2010.12.007.

[15] Rossetti, I.; Lassoa, J.; Nichele, V.; Signoretto, M.; Finocchio, E.; Ramis, G.; Di Michele, A. Silica and zirconia supported catalysts for the low-temperature ethanol steam reforming. Appl. Catal., B 2014, 150–151, 257–267, DOI 10.1016/j.apcatb.2013.12.012.

[16] Rossetti, I.; Gallo, A.; Santo, V.D.; Bianchi, C.L.; Nichele, V.; Signoretto, M.; Finocchio, E.; Ramis, G.; Di Michele, A. Nickel catalysts supported over TiO_2, SiO_2 and ZrO_2 for steam reforming of glycerol. ChemCatChem 2013, 5, 294 – 306, DOI 10.1002/cctc.201200481.

[17] Nichele, V.; Signoretto, M.; Menegazzo, F.; Gallo, A.; Santo, V. D.; Cruciani, G.; Cerrato, G. Glycerol steam reforming for hydrogen production: Design of Ni supported catalysts. Appl. Catal., B 2012, 111–112, 225–232, DOI 10.1002/cctc.201200481.

[18] Montini, T.; Melchionna, M.; Monai, M.; Fornasiero, P. Fundamentals and Catalytic Applications of CeO_2-Based Materials. Chem. Rev. 2016, 116, 5987−6041, DOI 10.1021/acs.chemrev.5b00603.

[19] Capdevila-Cortada, M.; Vilé, G.; Teschner, D.; Pérez-Ramírez, J.; López, N. Reactivity descriptors for ceria in catalysis. Appl. Catal., B 2016, 197, 299–312, DOI 10.1016/j.apcatb.2016.02.035.

[20] Reina, T.R.; Ivanova, S.; Idalkiev, V. ; Tabakova, T.; Centeno, M.A.; Deng, Q. ; Yuan, Z. ; Odriozola, J.A. Nanogold mesoporous iron promoted ceria catalysts for total and preferential CO oxidation reactions. J. Mol. Catal. A: Chem 2016, 414, 62-71, DOI 10.1016/j.molcata.2016.01.003.

[21] Mullins, D. R. The surface chemistry of cerium oxide. Surf. Sci. Rep. 2015, 70, 42–85, DOI 10.1016/j.surfrep.2014.12.001.

[22] Rotaru, C.G.; Postole, G.; Florea, M.; Matei-Rutkovska, F.; Parvulescu, V.I.; Gelin, P. Dry reforming of methane on ceria prepared by modified precipitation route. Appl. Catal., A 2015, 494, 29-40, DOI 10.1016/j.apcata.2015.01.024.

[23] Laguna, O.H.; Centeno, M.A.; Boutonnet, M. J.; Odriozola, A. Au-supported on Fe-doped ceria solids prepared in water-in-oil microemulsions catalysts for CO oxidation. Catal. Today 2016, 278, 140–149, DOI 10.1016/j.cattod.2016.05.059.

[24] Andana, T.; Piumetti, M.; Bensaid, S.; Veyre, L.; Thieuleux, C.; Russo, N.; Fino, D.; Quadrelli, E.A.; Pirone, R. Ceria-supported small Pt and Pt_3Sn nanoparticles for NO_x-assisted soot oxidation. Appl. Catal., B 2017, 209, 295-310, DOI 10.1016/j.apcatb.2017.03.010.

[25] Liu, F.; Zhao, L.; Wang, H.; Bai, X.; Liu, Y. Study on the preparation of Ni-La-Ce oxide catalyst for steam reforming of ethanol. Int. J. Hydrogen Energy 2014, 39, 10454-10466, DOI 10.1016/j.ijhydene.2014.05.036.

[26] Cao, J.; Wang, Y.; Zhang, T.; Wu, S.; Yuan., Z. Preparation, characterization and catalytic behavior of nanostructured mesoporous CuO/Ce0. 8Zr0. 2O2 catalysts for low-temperature CO oxidation. Appl. Catal., B 2008, 78, 120-128, DOI 10.1016/j.apcatb.2007.09.007.

[27] Venezia, A.M.; Parola, V.L.; Liotta, L.F. Structural and surface properties of heterogeneous catalysts: Nature of the oxide carrier and supported particle size effects. Catal. Today 2017, 285, 114–124, DOI 10.1016/j.cattod.2016.11.004.

[28] Omoregbe, O.; Danh, H.T.; Abidin, S.Z.; Setiabudi, H.D.; Abdullah, B.; Vu, K.B.; Vo, D.N. Influence of Lanthanide Promoters on Ni/SBA-15 Catalysts for Syngas Production by Methane Dry Reforming, Procedia Eng. 2016, 148, 1388 – 1395, DOI 10.1016/j.proeng.2016.06.556.

[29] Ideris, A.; Croiset, E.; Pritzker, M.; Amin, A. Direct-methane solid oxide fuel cell (SOFC) with Ni-SDC anode-supported cell. Int. J. Hydrogen Energy 2017, 42, 23118-2312, DOI 10.1016/j.ijhydene.2017.07.117.

[30] Idriss, H.; Diagne, C.; Hindermann, J.P.; Kiennemann, A.; Barteau, M.A. Reactions of acetaldehyde on CeO_2 and CeO_2-supported catalysts. J. Catal. 1995, 155, 219-237, DOI 10.1006/jcat.1995.1205.

[31] Moraes, T.S.; Rabelo Neto, R.C.; Ribeiro, M.C.; Mattos, L.V.; Kourtelesis, M.; Ladas, S.; Verykios, X.; Noronha, F.B. Ethanol conversion at low temperature over CeO_2—Supported Ni-based catalysts. Effect of Pt addition to Ni catalyst. Appl. Catal., B 2016, 181, 754-768, DOI 10.1016/j.apcatb.2015.08.044.

[32] Ochoa, J.V.; Trevisanut, C.; Millet, J.M.; Busca, G.; Cavani, F.; In situ DRIFTS-MS study of the anaerobic oxidation of ethanol over spinel mixed oxides. J. Phys. Chem. 2013, 117, 23908-23918, DOI 10.1021/jp409831t.

[33] Xu, W.; Liu, Z.; Johnston-Peck, A.C.; Senanayake, S.D.; Zhou, G.; Stacchiola, D.; Stach, E.A.; Rodriguez, J.A. Steam Reforming of Ethanol on Ni/CeO2: Reaction Pathway and Interaction between Ni and the CeO2 Support. ACS Catal. 2015, 3, 975-984, DOI 10.1021/cs4000969.

[34] Seiferth, O.; Wolter, K.; Dillmann, B.; Klivenyi, G.; Freund, H. J.; Scarano, D.; Zecchina, A. IR investigations of CO2 adsorption on chromia surfaces: Cr_2O_3 (0001)/Cr(110) versus polycrystalline α-Cr_2O_3. Surf. Sci. 1999, 412, 176-190, DOI 10.1016/S0039-6028(98)00857-7.

[35] Busca, G. The use of vibrational spectroscopies in studies of heterogeneous catalysis by metal oxides: an introduction. Catal. Today 1996, 27, 323-352, DOI 10.1016/0920-5861(96)88647-0.

[36] Zhang, R.; Lu, K.; Zong, L.; Tong, S.; Wang, X.; Feng, G. Gold supported on ceria nanotubes for CO oxidation. Appl. Surf. Sci. 2017, 416, 183–190, DOI 10.1016/j.apsusc.2017.04.158.

[37] Collins, S.; Finos, G.; Alcantara, R.; del Rio, E.; Bernal, S.; Bonivardi, A.; Effect of gallia doping on the acid–base and redox properties of ceria. Appl. Catal., A 2010, 388, 202–210, DOI 10.1016/j.apcata.2010.08.050.

[38] Dong, W.; Roh, H.; Jun, K.; Park, S.; Oh, Y. Methane reforming over Ni/Ce-ZrO2 catalysts: effect of nickel content. Appl. Catal., A 2002, 226, 63–72, DOI 10.1016/S0926-860X(01)00883-3.

[39] Marrero-Jerez, J.; Larrondo, S.; Rodríguez-Castellón, E.; Núñez, P. TPR, XRD and XPS characterisation of ceria-based materials synthesized by freeze-drying precursor method. Ceram. Int. 2014, 40, 6807–6814, DOI 10.1016/j.ceramint.2013.11.143.

[40] Mandapaka, R.; Madras, G. Aluminium and rhodium co-doped ceria for water gas shift reaction and CO oxidation. Mol. Catal. 2018, 451, 4-12, DOI 10.1016/j.mcat.2017.10.001.

[41] Glass, D. E.; Galvan, V.; Prakash, G.K. S. The Effect of Annealing Temperature on Nickel on Reduced Graphene Oxide Catalysts on Urea Electrooxidation. Electrochim. Acta 2017, 253, 489–497, DOI 10.1016/j.electacta.2017.09.064.

[42] Centi, G.; Perathoner, S. Opportunities and prospects in the chemical recycling of carbon dioxide to fuels. Catal. Today 2009, 148, 191-205, DOI 10.1016/j.cattod.2009.07.075.

[43] Gonzalez-DelaCruz, V.M.; Holgado, J.P.; Perenìguez, R.; Caballero, A. Morphology changes induced by strong metal–support interaction on a Ni–ceria catalytic system. J. Catal. 2008, 257, 307-314, DOI 10.1016/j.jcat.2008.05.009

[44] Brunauer, S.; Emmett, P. H.; Teller E. Adsorption of Gases in Multimolecular Layers. J. Am. Chem. Soc. 1938, 60, 309-319.

[45] Barrett, E. P.; Joyner, L. S.; Halenda, P. P. The Determination of Pore Volume and Area Distributions in Porous Substances. I. Computations from Nitrogen Isotherms, J. Am. Chem. Soc. 1951, 73, 373-380.

TOC

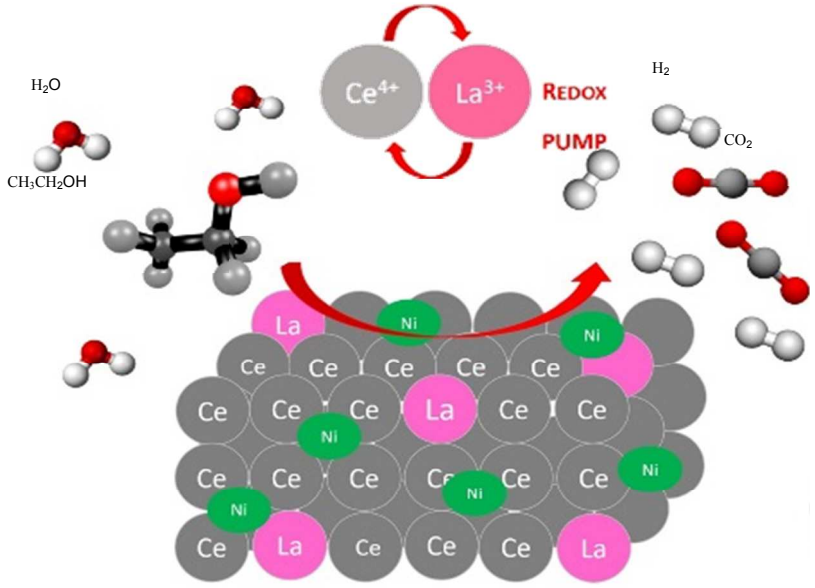

SYNOPSIS

Development of new lanthanum doped Ni/CeO_2 catalysts for the production of the energy carrier of the future.